Robotica (2022), **40**, pp. 3136–3156
doi:10.1017/S0263574722000108

CAMBRIDGE
UNIVERSITY PRESS

REPLY

Time delay estimation-based reactionless augmented adaptive sliding mode control of a space manipulator's pregrasping a target

Xiaoyan Yu[1,2,*], Jianqiao Guo[1,*] and Jianyu Zhang[1]

[1]School of Mechanical Engineering and Automation, Fuzhou University, Fuzhou 350116, China and [2]Key Laboratory of Fluid Power and Intelligent Electro-Hydraulic Control, (Fuzhou University), Fujian Province University, Fuzhou 350116, China
*Corresponding author. E-mail: cool09@163.com

Received: 12 August 2021; **Revised:** 6 January 2022; **Accepted:** 10 January 2022; **First published online:** 11 March 2022

Keywords: reaction null space, free-floating manipulator, motion planning, time delay estimation, augmented adaptive sliding mode control

Abstract

Reaction null space (RNS) planning and control of a planar three-link space manipulator's pregrasping a spinning target are studied. First, the Lagrange dynamic model of the manipulator was established. Second, the RNS motion planning algorithm was derived, and the vector norm constraint algorithm of RNS planning was addressed to ensure certain joint angular acceleration constraints were satisfied. Furthermore, an augmented adaptive sliding mode controller based on time delay estimation (TDE) was proposed. This controller estimated the unknowns of the system by TDE technology, in which accurate and complete dynamics were not required, and an adaptive TDE was introduced to decrease the estimation errors and avoid serious chattering. Finally, numerical simulations were carried out to verify the effectiveness of the proposed RNS planning and control algorithm.

1. Introduction

With the development of space technology, space manipulator has been used more and more widely [1, 2, 3]. Due to space microgravity, there are strong couplings between the base and the arm. The reaction forces and torques onto the base caused by the space manipulator lead to the translation motions and rotations of the base, which in turn affect the manipulation performances of the arm. In order to guarantee better navigation and communication signal, as well as ensure the solar panels work, certain attitudes of the base need to be kept. Attitudes of the base can usually be controlled by the active attitude control system (ACS) [4, 5, 6, 7]. However, the ACS sometimes needs to be shut down to avoid collisions between the gripper of the manipulator and the handle of the target during the sudden firing of the thrusters, as well as to conserve fuel. So other techniques are required.

Dubowskys et al. [8, 9] proposed an enhanced disturbance map (EDM) based joint motion planning strategy to reduce the attitude disturbance of the base caused by the manipulator motion. By a fixed-attitude-restrict Jacobian matrix (FARJM) based technique, Nenchev et al. [10] conducted zero-disturbance planning of a space manipulator. Furthermore, Yoshida et al. [11] addressed the redundant degree of freedom of the space manipulator and realized zero reaction maneuver (ZRM) by introducing a combined matrix [12, 13]. To the dynamic uncertain system, Nguyen Huynh et al. [14] investigated the base attitude zero disturbance while the arms moved. And Xu et al. [15] studied a reactionless adaptive kinematics controller to ensure the base's attitude controlled and the end-effector to track the desired trajectory. Zong et al. [16] presented a new dynamic formulation as well as control scheme for space manipulators to assure the end-effector to track a desired trajectory and to minimize the base disturbances caused by the arm movements, in which joint controllers were designed without solving for the inverse kinematics and computing the derivative of the generalized Jacobian matrix.

© The Author(s), 2022. Published by Cambridge University Press.

https://doi.org/10.1017/S0263574722000108 Published online by Cambridge University Press

Sliding mode control can be applied to control space manipulators [17, 18, 19], in which there are structured uncertainty (and) or unstructured uncertainty [20]. Moreover, diverse sliding surfaces were designed [17, 21, 22, 23], and different sliding mode controllers (SMC) were proposed. Bayat [24] combined nonlinear terminal sliding mode control (TSMC) and linear model predictive control (MPC) in a compound double layer structure to deal with the robust optimal three-axis attitude tracking problem of spacecraft. Shao et al. [25] proposed a nonsingular terminal sliding mode controller (NTSMC) for free-floating space manipulators (FFSMs) to improve the transient performance and reduce unexpected base motion in the presence of disturbance. Zhu et al. [26] investigated the precise and fast trajectory tracking controller for the free-flying space manipulator, after capturing a space target with uncertain mass, and proposed a novel adaptive sliding mode disturbance observer (ASMDO) which assured the estimation error of ASMDO stabilized in finite-time with the bound of the derivative of system uncertainty unknown. Since the time delay estimation (TDE) technique was proposed, more attention is paid to the TDE-based controller (TDEC) for its low dependence on the dynamics model [27, 28, 29, 30]. However, without taking the compensation of the TDE error into account, there is serious chattering in SMC [28]. Lee [31] et al. made an experimental study on time delay control of actuation system of tilt rotor unmanned aerial vehicle. TDE techniques were studied and SMC based on TDE of terrestrial manipulators were proposed [32, 33]. Jung et al. [34] demonstrated the structural equivalence between a nonlinear disturbance observer and a time-delay controller (TDC) under the non-model-based control framework of terrestrial manipulators. Zhang [35] et al. addressed an adaptive fuzzy SMC to control a free-flying space manipulator. Liang [36] studied a fuzzy wavelet neural network sliding mode controller for a free-flying flexible joint double-arm space robot based on TDE. And Xie et al. [37] presented a new adaptive small chattering sliding mode control (SCSMC) scheme that uses reinforcement learning (RL) and time-delay estimation (TDE) for the motion control of free-floating space robotic manipulators (FSRM) subject to model uncertainty and external disturbance.

The motion planning strategies [7, 8, 9, 10, 11, 12, 13, 14, 15, 16] were mainly devoted to general operations of space manipulations, which cannot apply to cases of a space manipulator's pregrasping a spinning target. Furthermore, there are no limits and restrictions of the joint angular accelerations, which need to be considered to accommodate the actual working situations. And in the TDE-based controllers [31, 32, 33, 34], a fixed inertial matrix estimate is adopted all the time, which may lead to degradation of the controller for a time-varying task. In this work, RNS planning and control of a planar three-link space manipulator's pregrasping a spinning target are studied. First, the Lagrange dynamic model of the manipulator was established. Second, the RNS motion planning algorithm was derived, and the vector norm constraint algorithm of RNS planning was addressed to ensure certain joint angular acceleration constraints were satisfied. Furthermore, an augmented adaptive sliding mode control algorithm based on TDE was proposed. This algorithm estimated the unknowns by TDE technology, in which accurate and complete dynamics were not required. An adaptive TDE was introduced to decrease the estimation errors and avoid serious chattering. Finally, numerical simulations were carried out to verify the effectiveness of the proposed RNS planning and control algorithm.

2. Dynamic modeling of space manipulators

A planar three-link space manipulator and a spinning target are shown in Fig. 1. The space manipulator consists of a free-floating rigid base B_0 (chaser) and rigid bars B_1, B_2, B_3. P is the target to be captured. Oxy is the inertial coordinate frame of the system. And the base moves along its trajectory with a velocity $\boldsymbol{v}$. It is assumed that the mass center of the whole system and that of the base satellite coincide for any configuration of the manipulator [38]. Due to the large radius of curvature of the trajectory, the trajectory in a short period can be approximately regarded as a straight line. The target is a cylindrical object revolving around its mass center with angular velocity $\dot{\theta}_p$, and the distance between its handle and its mass center is r_{h}. The trajectory of the base is inclined at an angle ψ relative to the x axis, and the distance between the mass center of the target and the base's trajectory is d. At the point of interception, the relative velocity between the manipulator end-effector and the handle of the target is $\Delta\boldsymbol{v}$. $O_i x_i y_i$ is the local coordinate frame of $B_i (i = 0, 1, 2, 3)$. O_0 is coincident with the mass center $O_{\mathrm{c}0}$ of B_0, O_{ci} is the

https://doi.org/10.1017/S0263574722000108 Published online by Cambridge University Press

mass center of $B_i(i = 0, 1, 2, 3)$, $O_i(i = 1, 2, 3)$ is the rotational center of the revolute joint between B_{i-1} and $B_i(i = 0, 1, 2, 3)$, $x_i(i = 1, 2, 3)$ is the symmetry axis of B_i, respectively. Other symbols are defined as follows:

$\boldsymbol{e}_i$ Unit vector along the x_i axis;
l_0 Distance between points O_0 and O_1;
l_i Length of B_i (i = 1,2,3) along the x_i axis;
b_i Distance between point $O_i(i = 1, 2, 3)$ and the mass center O_{Ci} (i = 1,2,3);
m_i Mass of B_i (i = 0,1,2,3);
J_i Inertial moment of B_i with respect to its mass center O_{Ci} (i = 0,1,2,3);
O_c Mass center of the system;
θ_0 Attitude angle of x_0 axis relative to x axis;
θ_i Joint angles of B_i (i = 1,2,3);
$\boldsymbol{r}_i$ Position vector of the mass center O_{Ci} of B_i (i = 0,1,2,3) in (O-xy) frame, $r_i = [x_i \quad y_i]^{\mathrm{T}}$;
T_i The kinetic energy of B_i (i = 0,1,2,3)
$\dot{(\,)}$ The first time derivative of ( );
$\ddot{(\,)}$ The second time derivative of ( );
$\hat{(\,)}$ The estimate of ( );
$[(\,)]$ The allowable value of ( ).

From Fig. 1, $\boldsymbol{r}_i$ (i = 1,2,3) are

$$\boldsymbol{r}_i = \boldsymbol{r}_0 + \sum_{j=0}^{i-1} l_j \boldsymbol{e}_j + b_i \boldsymbol{e}_i \tag{1}$$

Differentiating Eq. (1) with respect to time t, $\dot{\boldsymbol{r}}_i$ (i = 1,2,3) are

$$\dot{\boldsymbol{r}}_i = \dot{\boldsymbol{r}}_0 + \sum_{j=0}^{i-1} l_j \dot{\boldsymbol{e}}_j + b_i \dot{\boldsymbol{e}}_i \tag{2}$$

Then the manipulator system's total kinetic energy T is

$$T = \sum_{i=0}^{3} T_i \tag{3}$$

where $T_i = \dfrac{1}{2}\left(m_i \dot{\boldsymbol{r}}_i^2 + J_i\left(\sum_{j=0}^{i} \dot{\theta}_j\right)^2\right)$.

The microgravity is ignored, and the potential energy of the system V is 0. Then the system's Lagrangian $L = T$-V= T and the Euler–Lagrange dynamic equations of the space manipulator are derived as [39]

$$\boldsymbol{D}(\boldsymbol{q})\ddot{\boldsymbol{q}} + \boldsymbol{H}(\boldsymbol{q}, \dot{\boldsymbol{q}})\dot{\boldsymbol{q}} = \boldsymbol{\tau} \tag{4}$$

where $\boldsymbol{q} = [x_0 \quad y_0 \quad \theta_0 \quad \theta_1 \quad \theta_2 \quad \theta_3]^{\mathrm{T}}$ is the generalized coordinates, $\boldsymbol{D}(\boldsymbol{q}) \in \boldsymbol{R}^{6\times6}$ denotes the symmetric inertial matrix, $\boldsymbol{H}(\boldsymbol{q}, \dot{\boldsymbol{q}}) \in \boldsymbol{R}^{6\times6}$ is the Coriolis/centrifugal matrix, $\boldsymbol{\tau} = \begin{bmatrix}\boldsymbol{0} & \boldsymbol{\tau}_l^{\mathrm{T}}\end{bmatrix}^{\mathrm{T}} \in \boldsymbol{R}^{6\times1}$, $\boldsymbol{\tau}_l = [\tau_1 \quad \tau_2 \quad \tau_3]^{\mathrm{T}} \in \boldsymbol{R}^{3\times1}$, $\tau_i(i = 1, 2, 3)$ is the input torque of joint i.

https://doi.org/10.1017/S0263574722000108 Published online by Cambridge University Press

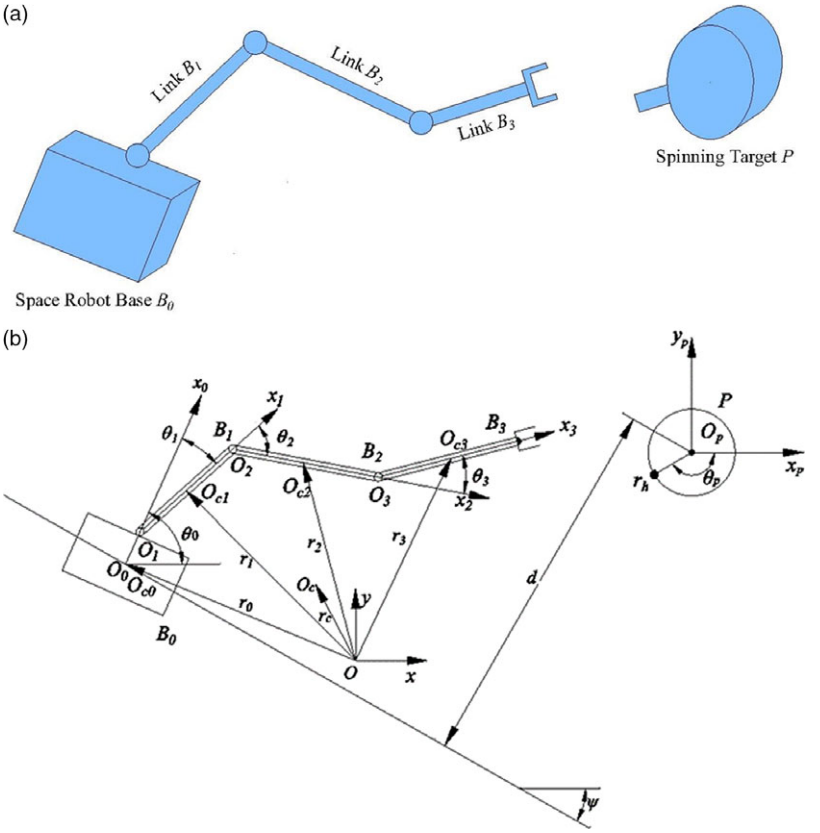


Figure 1. *A free-floating space manipulator and a spinning target.*

3. RNS motion planning of space manipulators

3.1. RNS motion planning algorithm

By partitioned matrix, Eq. (4) is rewritten as

$$\begin{bmatrix} \boldsymbol{D}_{bb} & \boldsymbol{D}_{bl} \\ \boldsymbol{D}_{lb} & \boldsymbol{D}_{ll} \end{bmatrix} \begin{bmatrix} \ddot{\boldsymbol{q}}_b \\ \ddot{\boldsymbol{q}}_l \end{bmatrix} + \begin{bmatrix} \boldsymbol{H}_b \\ \boldsymbol{H}_l \end{bmatrix} \begin{bmatrix} \dot{\boldsymbol{q}}_b \\ \dot{\boldsymbol{q}}_l \end{bmatrix} = \begin{bmatrix} \boldsymbol{0} \\ \boldsymbol{\tau}_l \end{bmatrix} \tag{5}$$

where $\boldsymbol{D}_{bb} \in \boldsymbol{R}^{3\times3}$ is the base inertia matrix, $\boldsymbol{D}_{ll} \in \boldsymbol{R}^{3\times3}$ is the arm inertial matrix, $\boldsymbol{D}_{bl} \in \boldsymbol{R}^{3\times3}$ is the base-arm coupling inertia matrix, $\boldsymbol{q}_b = [x_0 \quad y_0 \quad \theta_0]^{\mathrm{T}}$, $\boldsymbol{q}_l = [\theta_1 \quad \theta_2 \quad \theta_3]^{\mathrm{T}}$.

Integrating the first row of Eq. (5), the system's linear momentum $\boldsymbol{P}$ and angular momentum $\boldsymbol{L}$ [40] are

$$\begin{pmatrix} \boldsymbol{P} \\ \boldsymbol{L} \end{pmatrix} = \int \boldsymbol{0} dt = \boldsymbol{D}_{bb}\dot{\boldsymbol{q}}_b + \boldsymbol{D}_{bl}\dot{\boldsymbol{q}}_l = const \tag{6}$$

where $\boldsymbol{D}_{bb}\dot{\boldsymbol{q}}_b$ is the base momentum, $\boldsymbol{D}_{bl}\dot{\boldsymbol{q}}_l$ is the coupling momentum generated by the arm motion. Introduce $\boldsymbol{L}_l = \boldsymbol{D}_{bl}\dot{\boldsymbol{q}}_l$ and the derivative of $\boldsymbol{L}_l$ is

$$\dot{\boldsymbol{L}}_l = \boldsymbol{F}_l = \boldsymbol{D}_{bl}\ddot{\boldsymbol{q}}_l + \dot{\boldsymbol{D}}_{bl}\dot{\boldsymbol{q}}_l \tag{7}$$

where $\boldsymbol{F}_l$ is the reaction forces induced on the base from the motion of the arm.

https://doi.org/10.1017/S0263574722000108 Published online by Cambridge University Press

When coupling momentum is constant, $\boldsymbol{F}_l \equiv \boldsymbol{0}$. Then the arm's motion leads to no reaction force or torque to the base. When the number of the degree of freedom of the manipulator is greater than that of the base coordinates, the manipulator joint rates satisfy [40]

$$\dot{\boldsymbol{q}}_l = \boldsymbol{D}_{bl}^{+}\boldsymbol{L}_l + \left(\boldsymbol{I} - \boldsymbol{D}_{bl}^{+}\boldsymbol{D}_{bl}\right)\boldsymbol{\xi} \tag{8}$$

where $(\,)^{+}$ is the pseudo-inverse of $(\,)$, $\boldsymbol{I} \in \boldsymbol{R}^{3\times 3}$ represents the identity matrix, $(\boldsymbol{I} - \boldsymbol{D}_{bl}^{+}\boldsymbol{D}_{bl})$ is the mapping onto the null space of $\boldsymbol{D}_{bl}$, and $\boldsymbol{\xi} \in \boldsymbol{R}^{3\times 1}$ represents an arbitrary vector. This inertial null space is called the "zero reaction space." When the coupling momentum $\boldsymbol{L}_l = \boldsymbol{0}$, Eq. (9) is obtained

$$\left(\dot{\boldsymbol{q}}_l\right)_{RNS} = \left(\boldsymbol{I} - \boldsymbol{D}_{bl}^{+}\boldsymbol{D}_{bl}\right)\boldsymbol{\xi} \tag{9}$$

The base's attitude is merely considered and the modified coupling inertial matrix $\tilde{\boldsymbol{D}}_{bl} = [D_{34}\ \ D_{35}\ \ D_{36}]$ [32] is defined, then Eq. (9) is transformed into

$$\left(\dot{\boldsymbol{q}}_l\right)_{RNS} = \left(\boldsymbol{I} - \tilde{\boldsymbol{D}}_{bl}^{+}\tilde{\boldsymbol{D}}_{bl}\right)\boldsymbol{\xi} \tag{10}$$

The reactionless joint trajectories can be obtained by integrating Eq. (10).

3.2. Vector norm constraint algorithm of RNS planning

$\boldsymbol{\xi}$ can be properly chosen to ensure constraints of the joint angular velocities and joint angular accelerations are satisfied. Define $\boldsymbol{B} = (\boldsymbol{I} - \tilde{\boldsymbol{D}}_{bl}^{+}\tilde{\boldsymbol{D}}_{bl})$ and utilize Eq. (10), joint angular velocities $\left(\dot{\boldsymbol{q}}_l\right)_{int}$ and joint angular accelerations $\left(\ddot{\boldsymbol{q}}_l\right)_{int}$ at the interception point are

$$\begin{cases} \left\| \left(\dot{\boldsymbol{q}}_l\right)_{int} \right\| = \|\boldsymbol{B}\boldsymbol{\xi}\| \\ \left\| \left(\ddot{\boldsymbol{q}}_l\right)_{int} \right\| = \left\| \dfrac{d\boldsymbol{B}}{dt}\boldsymbol{\xi} \right\| \end{cases} \tag{11}$$

Extending it to the entire manipulation process, then joint angular velocities $(\dot{\boldsymbol{q}}_l)_{RNS}$ and joint angular accelerations $(\ddot{\boldsymbol{q}}_l)_{RNS}$ of RNS are

$$\begin{cases} \left\| \left(\dot{\boldsymbol{q}}_l\right)_{RNS} \right\| = \|\boldsymbol{B}\boldsymbol{\xi}\| \\ \left\| \left(\ddot{\boldsymbol{q}}_l\right)_{RNS} \right\| = \left\| \dfrac{d\boldsymbol{B}}{dt}\boldsymbol{\xi} \right\| \end{cases} \tag{12}$$

By Eq. (7), the reaction forces onto the base from the arm are

$$\boldsymbol{F}_{RNS} = \boldsymbol{D}_{bl}\left(\ddot{\boldsymbol{q}}_l\right)_{RNS} + \dot{\boldsymbol{D}}_{bl}\left(\dot{\boldsymbol{q}}_l\right)_{RNS} = \begin{pmatrix} F_x \\ F_y \\ T_z \end{pmatrix} \tag{13}$$

where F_x and F_y are reaction forces, T_z is the corresponding reaction torque.

Substituting $\left(\dot{\boldsymbol{q}}_l\right)_{RNS} = \boldsymbol{B}\boldsymbol{\xi}$ and $\left(\ddot{\boldsymbol{q}}_l\right)_{RNS} = \dfrac{d\boldsymbol{B}}{dt}\boldsymbol{\xi}$ into Eq. (13), then combining Eq. (12), Eq. (14) is derived

$$\begin{cases} \left\| \left(\dot{\boldsymbol{q}}_l\right)_{RNS} \right\|_2 = \|\boldsymbol{B}\boldsymbol{\xi}\|_2 \\ \left\| \left(\ddot{\boldsymbol{q}}_l\right)_{RNS} \right\|_2 = \left\| \dfrac{d\boldsymbol{B}}{dt}\boldsymbol{\xi} \right\|_2 \\ \|\boldsymbol{F}_{RNS}\|_2 = \left\| \left(\boldsymbol{D}_{bl}\dfrac{d\boldsymbol{B}}{dt} + \dot{\boldsymbol{D}}_{bl}\boldsymbol{B}\right)\boldsymbol{\xi} \right\|_2 \end{cases} \tag{14}$$

https://doi.org/10.1017/S0263574722000108 Published online by Cambridge University Press

where $\|\|_2$ is the Euclidean norm. Then

$$\begin{cases} \left\| \left(\dot{\boldsymbol{q}}_l \right)_{RNS} \right\|_2^2 = \boldsymbol{\xi}^{\mathrm{T}} \boldsymbol{A}_1 \boldsymbol{\xi} \\ \left\| \left(\ddot{\boldsymbol{q}}_l \right)_{RNS} \right\|_2^2 = \boldsymbol{\xi}^{\mathrm{T}} \boldsymbol{A}_2 \boldsymbol{\xi} \\ \left\| \boldsymbol{F}_{RNS} \right\|_2^2 = \boldsymbol{\xi}^{\mathrm{T}} \boldsymbol{A}_3 \boldsymbol{\xi} \end{cases} \tag{15}$$

where $\boldsymbol{A}_i \in \boldsymbol{R}^{3\times 3} (i = 1, 2, 3)$ are obtained by expanding the right side of Eq. (14). Then $\boldsymbol{\xi}$ can be calculated by Eq. (15).

The reactionless path of the manipulator can be obtained by integrating Eq. (10) from t_f to t_0, in which t_f is the time of interception and t_0 is the starting time of manipulation. The initial states of the integral are joint angles of the manipulator at the moment of interception, which should be obtained first. This can be obtained by inverse kinematics [39].

At the moment of interception, the velocity $\boldsymbol{v}_e$ of the end-effector should be the same as the velocity $\boldsymbol{v}_h$ of the target handle. In practice, $\|\boldsymbol{v}_e - \boldsymbol{v}_h\| \leq [\Delta v]$ is ensured. The end-effector's velocity is

$$\boldsymbol{v}_e = \boldsymbol{v}_{O0} + \boldsymbol{v}_{eO0} \tag{16}$$

where $\boldsymbol{v}_{O0}$ is the velocity of O_0, $\boldsymbol{v}_{eO0}$ is the relative velocity of the end-effector relative to O_0.

$$\boldsymbol{v}_{eO0} = \boldsymbol{J} \dot{\boldsymbol{q}}_\theta \tag{17}$$

where $\dot{\boldsymbol{q}}_\theta = [\dot{\theta}_0 \quad \dot{\theta}_1 \quad \dot{\theta}_2 \quad \dot{\theta}_3]^{\mathrm{T}}$, $\boldsymbol{J}$ is Jacobian matrix.

$$\boldsymbol{J} = \begin{bmatrix} -l_0 s_0 - l_l s_{01} - l_2 s_{012} - l_3 s_{0123} & -l_1 s_{01} - l_2 s_{012} - l_3 s_{0123} & -l_2 s_{012} - l_3 s_{0123} & -l_3 s_{0123} \\ l_0 c_0 + l_1 c_{01} + l_2 c_{012} + l_3 c_{0123} & l_1 c_{01} + l_2 c_{012} + l_3 c_{0123} & l_2 c_{012} + l_3 c_{0123} & l_3 c_{0123} \end{bmatrix} \tag{18}$$

where $s_0 = \sin(\theta_0)$, $s_{01} = \sin(\theta_0 + \theta_1)$, $s_{012} = \sin(\theta_0 + \theta_1 + \theta_2)$, $s_{0123} = \sin(\theta_0 + \theta_1 + \theta_2 + \theta_3)$, $c_0 = \cos(\theta_0)$, $c_{01} = \cos(\theta_0 + \theta_1)$, $c_{012} = \cos(\theta_0 + \theta_1 + \theta_2)$, $c_{0123} = \cos(\theta_0 + \theta_1 + \theta_2 + \theta_3)$.

The velocity $\boldsymbol{v}_h$ of the target handle is found from

$$\boldsymbol{v}_h = \begin{bmatrix} \dot{x}_h \\ \dot{y}_h \end{bmatrix} = \begin{bmatrix} \dot{x}_P - r_h \dot{\theta}_P \sin\theta_P \\ \dot{y}_P + r_h \dot{\theta}_P \cos\theta_P \end{bmatrix} \tag{19}$$

The main steps of the vector norm constraint algorithm of RNS Planning are shown in Fig. 2.

4. TDE-based augmented adaptive sliding mode control design

Introduce matrix $\boldsymbol{D}_l = \mathrm{diag}(D_{l1}, \cdots D_{li}, \cdots, D_{l6})$, the dynamics Eq. (4) is rewritten as

$$\boldsymbol{\tau} = \boldsymbol{D}_l \ddot{\boldsymbol{q}} + \boldsymbol{h} \tag{20}$$

$$\boldsymbol{h} = (\boldsymbol{D}(\boldsymbol{q}) - \boldsymbol{D}_l)\, \ddot{\boldsymbol{q}} + \boldsymbol{H}\,(\boldsymbol{q}, \dot{\boldsymbol{q}})\, \dot{\boldsymbol{q}} \tag{21}$$

where $\boldsymbol{D}_l$ is the estimate of the inertia matrix $\boldsymbol{D}$, $D_{li} (i = 1, \cdots, 6)$ are given constants.

Define the augmented output error vector

$$\boldsymbol{e} = \boldsymbol{q}_d - \boldsymbol{q} \tag{22}$$

$$\dot{\boldsymbol{e}} = \dot{\boldsymbol{q}}_d - \dot{\boldsymbol{q}} \tag{23}$$

where $\boldsymbol{q}_d = \begin{bmatrix} x_0 & y_0 & \theta_0 & \boldsymbol{q}_{ld}^{\mathrm{T}} \end{bmatrix}^{\mathrm{T}}$ and $\dot{\boldsymbol{q}}_d = \begin{bmatrix} \dot{x}_0 & \dot{y}_0 & \dot{\theta}_0 & \dot{\boldsymbol{q}}_{ld}^{\mathrm{T}} \end{bmatrix}^{\mathrm{T}}$ are the augmented desired trajectories and the augmented desired velocities, $\boldsymbol{q}_{ld} = [\theta_{1d} \quad \theta_{2d} \quad \theta_{3d}]^{\mathrm{T}}$, $\dot{\boldsymbol{q}}_{ld} = [\dot{\theta}_{1d} \quad \dot{\theta}_{2d} \quad \dot{\theta}_{3d}]^{\mathrm{T}}$. Then the augmented output error vector $\boldsymbol{e}$ is

$$\boldsymbol{e} = \begin{bmatrix} \boldsymbol{0} & \boldsymbol{e}_l^{\mathrm{T}} \end{bmatrix}^{\mathrm{T}} \tag{24}$$

where $\boldsymbol{e}_l = \boldsymbol{q}_{ld} - \boldsymbol{q}_l$.

https://doi.org/10.1017/S0263574722000108 Published online by Cambridge University Press

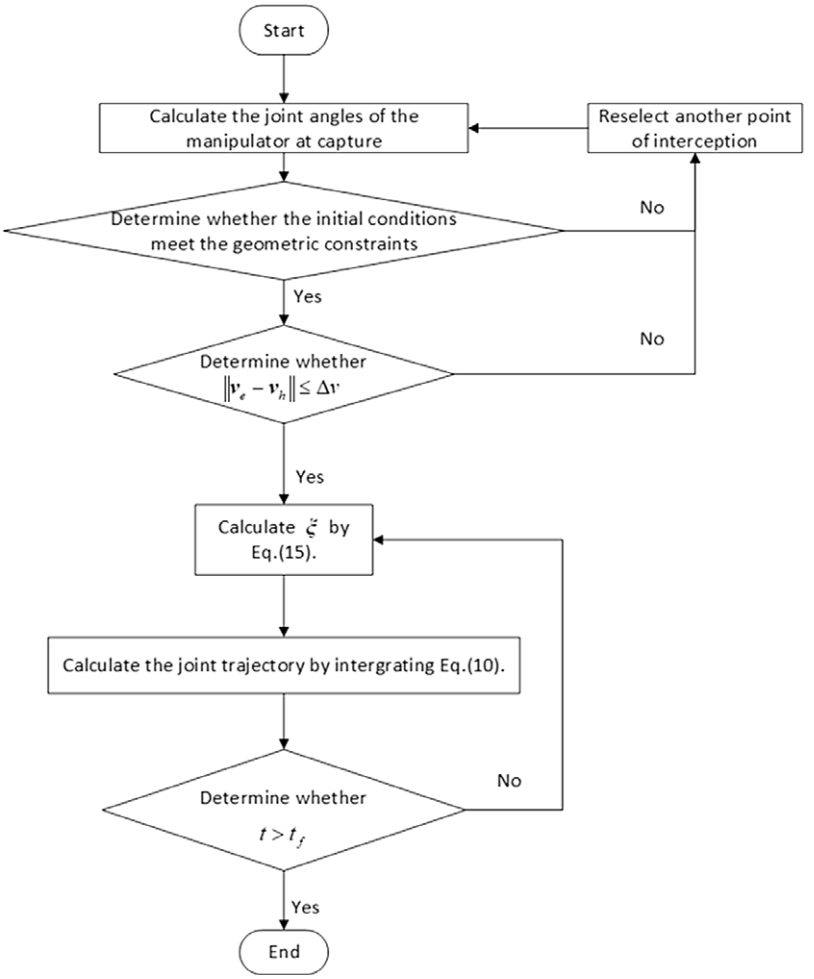


Figure 2. *The flow chart of the vector norm constraint algorithm of RNS planning.*

The sliding surface $\boldsymbol{s}$ is chosen as

$$\boldsymbol{s} = \dot{\boldsymbol{e}} + \boldsymbol{\Lambda}_1 \boldsymbol{e} + \boldsymbol{\Lambda}_2 \boldsymbol{\rho} \tag{25}$$

where $\boldsymbol{\Lambda}_1, \boldsymbol{\Lambda}_2 \in \boldsymbol{R}^{6\times 6}$ are positive definite diagonal matrices, $\boldsymbol{\Lambda}_1 = \mathrm{diag}(\lambda_{11}, \cdots, \lambda_{1i}, \cdots, \lambda_{16})$, $\boldsymbol{\Lambda}_2 = \mathrm{diag}(\lambda_{21}, \cdots, \lambda_{2i}, \cdots, \lambda_{26})$, $\lambda_{ji} > 0 (j = 1, 2; i = 1, \cdots, 6)$, $\boldsymbol{s} = [s_1 \ \cdots \ s_i \ \cdots \ s_6]^{\mathrm{T}}$, $\boldsymbol{\rho} = [\rho_1 \ \cdots \ \rho_i \ \cdots \ \rho_6]^{\mathrm{T}}$, $\rho_i (i = 1 \sim 6)$ are

$$\rho_i = \begin{cases} sig(e_i)^{\alpha_{1i}}, & s_{1i} = 0 \vee (s_{1i} \neq 0 \wedge |e_i| \geq \phi_i) \\ \eta_{1i} e_i + \eta_{2i} f(e_i), & s_{1i} \neq 0 \wedge |e_i| < \phi_i \end{cases} \tag{26}$$

$$f(e_i) = \left(1 + k_{1i} \cos\left(\frac{\pi e_i}{2\phi_i}\right)\right) sig(e_i)^{\alpha_{2i}} \tag{27}$$

where $s_{1i} = \dot{e}_i + \lambda_{1i} e_i + \lambda_{2i} sig(e_i)^{\alpha_{1i}}$, $0.5 < \alpha_{1i} < 1$, $1 < \alpha_{2i} < 2$, ϕ_i are positive constants, $sig(e_i)^{\alpha_{ji}} = |e_i|^{\alpha_{ji}} \mathrm{sgn}(e_i), j = 1, 2$, $\mathrm{sgn}(e_i)$, η_{1i} and η_{2i} are

$$\mathrm{sgn}(e_i) = \begin{cases} 1, & e_i > 0 \\ 0, & e_i = 0 \\ -1, & e_i < 0 \end{cases} \tag{28}$$

https://doi.org/10.1017/S0263574722000108 Published online by Cambridge University Press

$$\eta_{1i}=\left(\frac{\alpha_{2i}-\frac{\pi k_{1i}}{2}-\alpha_{1i}}{\alpha_{2i}-\frac{\pi k_{1i}}{2}-1}\right)\phi_i^{\alpha_{1i}-1},\ \eta_{2i}=\left(\frac{\alpha_{1i}-1}{\alpha_{2i}-\frac{\pi k_{1i}}{2}-1}\right)\phi_i^{\alpha_{1i}-\alpha_{2i}} \tag{29}$$

where $0\le k_{1i}<\dfrac{2(\alpha_{2i}-1)}{\pi}$.

The first time derivative of ρ_i is

$$\dot{\rho}_i=\begin{cases}\alpha_{1i}|e_i|^{\alpha_{1i}-1}\dot{e}_i, & s_{1i}=0\vee(s_{1i}\neq 0\wedge|e_i|\ge\phi_i)\\ \eta_{1i}\dot{e}_i+F(e_i)\ , & s_{1i}\neq 0\wedge|e_i|<\phi_i\end{cases} \tag{30}$$

$$F\left(e_i\right)=\eta_{2i}\alpha_{2i}\left(1+k_{1i}\cos\left(\frac{\pi e_i}{2\phi_i}\right)\right)|e_i|^{\alpha_{2i}-1}\dot{e}_i-\eta_{2i}k_{1i}\sin\left(\frac{\pi e_i}{2\phi_i}\right)sig(e_i)^{\alpha_{2i}}\frac{\pi\dot{e}_i}{2\phi_i} \tag{31}$$

Then the following approaching law $\boldsymbol{\Delta}$ is proposed

$$\boldsymbol{\Delta}=\boldsymbol{K}_1 s-\boldsymbol{K}_2 sig(\boldsymbol{s})^{\beta} \tag{32}$$

where $\boldsymbol{K}_1$ and $\boldsymbol{K}_2$ are diagonal matrices, $\boldsymbol{K}_1=\mathrm{diag}(\mu_{11},\cdots,\mu_{1i},\cdots,\mu_{16})$, $\boldsymbol{K}_2=\mathrm{diag}(\mu_{21},\cdots,\mu_{2i},\cdots,\mu_{26})$, $\mu_{ji}>0(j=1,2;i=1,\cdots,6)$, $0<\beta<1$.

By augmentation approach, an augmented sliding mode controller (controller I) is proposed

$$\boldsymbol{\tau}=\boldsymbol{D}_I\boldsymbol{\gamma}+\hat{\boldsymbol{h}}\left(\boldsymbol{q},\dot{\boldsymbol{q}},\ddot{\boldsymbol{q}}\right)+\left[\boldsymbol{\varsigma}^{\mathrm{T}}\quad\boldsymbol{0}\right] \tag{33}$$

$$\boldsymbol{\gamma}=\ddot{\boldsymbol{q}}_{\mathrm{d}}+\boldsymbol{w}+\boldsymbol{K}_1\boldsymbol{s}+\boldsymbol{K}_2 sig(\boldsymbol{s})^{\beta}+\boldsymbol{k}\,|\boldsymbol{w}|\,\mathrm{sgn}(\boldsymbol{s}) \tag{34}$$

where $\hat{\boldsymbol{h}}$ is the estimate of $\boldsymbol{h}$, $\boldsymbol{w}=\boldsymbol{\Lambda}_1\dot{\boldsymbol{e}}+\boldsymbol{\Lambda}_2\dot{\boldsymbol{\rho}}$, $\boldsymbol{w}=[w_1\quad\cdots\quad w_i\quad\cdots\quad w_6]^{\mathrm{T}}$, $\boldsymbol{k}=diag(k_1,\cdots,k_i,\cdots,k_6)$, $k_i(i=1\sim 6)$ is given later. The vector $\boldsymbol{\varsigma}=[\varsigma_1\ \ \varsigma_2\ \ \varsigma_3]^{\mathrm{T}}$ guarantees that the first three terms of the vector $\boldsymbol{\tau}=[\boldsymbol{0}\quad\boldsymbol{\tau}_l^{\mathrm{T}}]^{\mathrm{T}}$ are always 0.

By the adaptive delay estimation technique, $\hat{\boldsymbol{h}}(\boldsymbol{q},\dot{\boldsymbol{q}},\ddot{\boldsymbol{q}})$ is

$$\hat{\boldsymbol{h}}\left(\boldsymbol{q},\dot{\boldsymbol{q}},\ddot{\boldsymbol{q}}\right)=\boldsymbol{h}_{t-L}=\boldsymbol{\tau}_{t-L}-\boldsymbol{D}_l\ddot{\boldsymbol{q}}_{t-L} \tag{35}$$

As the delay time L is short enough, then

$$\boldsymbol{h}\approx\boldsymbol{h}_{t-L} \tag{36}$$

The acceleration $\ddot{\boldsymbol{q}}_{t-\mathrm{L}}$ is calculated by

$$\ddot{\boldsymbol{q}}_{t-L}=\frac{\boldsymbol{q}_t-2\boldsymbol{q}_{t-L}+\boldsymbol{q}_{t-2L}}{L^2} \tag{37}$$

The estimation error $\tilde{\boldsymbol{h}}_t$ is

$$\tilde{\boldsymbol{h}}_t=\boldsymbol{h}_t-\hat{\boldsymbol{h}}_t=\boldsymbol{h}_t-\boldsymbol{h}_{t-L}=\boldsymbol{D}_I\left(\boldsymbol{\gamma}-\ddot{\boldsymbol{q}}\right)+\left[\boldsymbol{\varsigma}^{\mathrm{T}}\quad\boldsymbol{0}\right] \tag{38}$$

Define the error $\boldsymbol{\delta}=[\delta_1\cdots\delta_i\cdots\delta_6]^{\mathrm{T}}$ as

$$\boldsymbol{\delta}=\boldsymbol{D}_I{}^{-1}\tilde{\boldsymbol{h}}_t=\boldsymbol{\gamma}-\ddot{\boldsymbol{q}}+\boldsymbol{D}_I^{-1}\left[\boldsymbol{\varsigma}^{\mathrm{T}}\quad\boldsymbol{0}\right] \tag{39}$$

So long as Eq. (40) is satisfied, the system is stable.

$$\left|\lambda_i\left(\boldsymbol{D}^{-1}\boldsymbol{D}_I-\boldsymbol{I}_6\right)\right|<1 \tag{40}$$

where $\boldsymbol{I}_6$ is a 6-dimensional identity matrix, $\lambda_i(\boldsymbol{D}^{-1}\boldsymbol{D_I}-\boldsymbol{I}_6)$ is the ith eigenvalue of the matrix $(\boldsymbol{D}^{-1}\boldsymbol{D_I}-\boldsymbol{I}_6)$, $i=1\sim 6$.

In order to decrease the TDE error, a larger constant needs to be chosen for D_{li} [41]. Larger D_{li} will lead to serious chattering. Even worse, Eq. (40) may not be satisfied, which leads to instabilities [29].

https://doi.org/10.1017/S0263574722000108 Published online by Cambridge University Press

Therefore, the adaptive TDE technology was introduced. Assume $\hat{\boldsymbol{D}} = \text{diag}(\hat{D}_1, \cdots, \hat{D}_i, \cdots, \hat{D}_6)$ is the adaptive estimated inertia matrix, the estimate $\hat{D}_i (i = 1 \sim 6)$ are

$$\hat{D}_i = D_{Ii} \left(1 + k_{2i}\sigma_i\right) \tag{41}$$

where $k_{2i} (i = 1 \sim 6)$ are positive constants, $\sigma_i (i = 1 \sim 6) \geq 0$ are defined later.

Then the augmented adaptive sliding mode controller based on TDE (controller II) is

$$\begin{aligned}\boldsymbol{\tau} &= \hat{\boldsymbol{D}}\boldsymbol{\gamma} + \hat{\boldsymbol{h}}\left(\boldsymbol{q}, \dot{\boldsymbol{q}}, \ddot{\boldsymbol{q}}\right) + \begin{bmatrix}\boldsymbol{\varsigma}^{\mathrm{T}} & \boldsymbol{0}\end{bmatrix} \\ &= \hat{\boldsymbol{D}}\left(\ddot{\boldsymbol{q}}_d + \boldsymbol{w} + \boldsymbol{K}_1\boldsymbol{s} + \boldsymbol{K}_2 sig(\boldsymbol{s})^{\beta}\right) + \hat{\boldsymbol{D}}\boldsymbol{k}\,|\boldsymbol{w}|\,\text{sgn}(\boldsymbol{s}) + \begin{bmatrix}\boldsymbol{\varsigma}^{\mathrm{T}} & \boldsymbol{0}\end{bmatrix} + \boldsymbol{\tau}_{t-L} - \hat{\boldsymbol{D}}\ddot{\boldsymbol{q}}_{t-L}\end{aligned} \tag{42}$$

Substituting Eq. (42) into Eq. (20), then we have

$$\ddot{\boldsymbol{q}} = \boldsymbol{D}_I^{-1}\left(\hat{\boldsymbol{D}}\boldsymbol{\gamma} + \hat{\boldsymbol{h}}(\boldsymbol{q}, \dot{\boldsymbol{q}}, \ddot{\boldsymbol{q}}) + \begin{bmatrix}\boldsymbol{\varsigma}^{\mathrm{T}} & \boldsymbol{0}\end{bmatrix} - \boldsymbol{h}\right) \tag{43}$$

Define the Lyapunov function V_i

$$V_i = \frac{1}{2}s_i^{\,2} + \frac{\tilde{\sigma}_i^2}{2\upsilon_i} \tag{44}$$

where υ_i is a positive constant, $\tilde{\sigma}_i = \sigma_{i,\max} - \sigma_i \geq 0$, $\sigma_{i,\max}$ is the maximum of σ_i, $i = 1 \sim 6$.

Differentiating Eq. (44) with respect to time t and utilizing $\boldsymbol{w} = \boldsymbol{\Lambda}_1\dot{\boldsymbol{e}} + \boldsymbol{\Lambda}_2\dot{\boldsymbol{\rho}}$, Eqs. (25) and (43), $\dot{V}_i$ is

$$\begin{aligned}\dot{V}_i &= s_i\dot{s}_i + \frac{\dot{\tilde{\sigma}}_i\tilde{\sigma}_i}{\upsilon_i} = s_i\left(\ddot{e}_i + \mu_{1i}\dot{e}_i + \mu_{2i}\dot{\rho}_i\right) + \frac{\dot{\tilde{\sigma}}_i\tilde{\sigma}_i}{\upsilon_i} = s_i\left(\ddot{q}_{id} - \ddot{q}_i + w_i\right) + \frac{\dot{\tilde{\sigma}}_i\tilde{\sigma}_i}{\upsilon_i} \\ &= \begin{cases} s_i\left(\ddot{q}_{id} - D_{Ii}^{-1}\left(\hat{D}_i\gamma_i + \hat{h}_i + \varsigma_i - h_i\right) + w_i\right) + \dfrac{\dot{\tilde{\sigma}}_i\tilde{\sigma}_i}{\upsilon_i} & i = 1, 2, 3 \\ s_i\left(\ddot{q}_{id} - D_{Ii}^{-1}\left(\hat{D}_i\gamma_i + \hat{h}_i - h_i\right) + w_i\right) + \dfrac{\dot{\tilde{\sigma}}_i\tilde{\sigma}_i}{\upsilon_i} & i = 4, 5, 6 \end{cases}\end{aligned} \tag{45}$$

$\sigma_{i,\max}$ is a constant and $\tilde{\sigma}_i = \sigma_{i,\max} - \sigma_i$, so $\dot{\tilde{\sigma}}_i = -\dot{\sigma}_i$. Define

$$\dot{\sigma}_i = \begin{cases} \upsilon_i\,|s_{2i}|\,\text{sgn}\left(\sigma_{i,\max} - \sigma_i\right), & \sigma_i = \sigma_{i,\max} \vee \sigma_i = 0 \\ \upsilon_i\,|s_{2i}|\,\text{sgn}\left(\chi_i - |s_i|^{\alpha_{3i}}\right), & 0 < \sigma_i < \sigma_{i,\max} \end{cases} \qquad i = 1 \sim 6 \tag{46}$$

where χ_i and υ_i are positive constants, $\alpha_{3i} > 1$. Then s_{2i} satisfies

$$|s_{2i}| = \begin{cases} |s_i|, & |s_i|^{\alpha_{3i}} > \chi_i \\ \left(|s_i| + \zeta_i\right)^{-1}, & |s_i|^{\alpha_{3i}} > \chi_i \end{cases} \qquad i = 1 \sim 6 \tag{47}$$

where ζ_i is a positive constant.

Then Eq. (47) is discussed by two situations. One is i = 1,2,3, the other is i = 4,5,6.

(1) i = 1,2,3

When i = 1,2,3, $s_i \equiv 0$. Then $\dot{V}_i$ is

$$\begin{aligned}\dot{V}_i &= \frac{\dot{\tilde{\sigma}}_i\tilde{\sigma}_i}{\upsilon_i} = -\frac{\dot{\sigma}_i\tilde{\sigma}_i}{\upsilon_i} \\ &= \begin{cases} -\,|s_{2i}|\,\text{sgn}\left(\sigma_{i,\max} - \sigma_i\right)\tilde{\sigma}_i, & \sigma_i = \sigma_{i,\max} \vee \sigma_i = 0 \\ -\,|s_{2i}|\,\text{sgn}\left(\chi_i - |s_i|^{\alpha_{3i}}\right)\tilde{\sigma}_i, & 0 < \sigma_i < \sigma_{i,\max} \end{cases} \qquad i = 1, 2, 3 \\ &= \begin{cases} -\left(|s_i| + \zeta_i\right)^{-1}\text{sgn}\left(\sigma_{i,\max} - \sigma_i\right)\tilde{\sigma}_i, & \sigma_i = \sigma_{i,\max} \vee \sigma_i = 0 \\ -\left(|s_i| + \zeta_i\right)^{-1}\text{sgn}\left(\chi_i - |s_i|^{\alpha_{3i}}\right)\tilde{\sigma}_i, & 0 < \sigma_i < \sigma_{i,\max} \end{cases} \\ &\leq 0\end{aligned} \tag{48}$$

https://doi.org/10.1017/S0263574722000108 Published online by Cambridge University Press

(2) $i = 4,5,6$

When $i = 4,5,6$, Eq. (49) is obtained by Eq. (39)

$$\begin{aligned}\dot{V}_i &= s_i\left(\ddot{q}_{id} - D_{Ii}^{-1}\left(\hat{D}_i\gamma_i + \tilde{h}_i\right) + w_i\right) + \frac{\dot{\tilde{\sigma}}_i\tilde{\sigma}_i}{\upsilon_i} \\ &= s_i\left(\ddot{q}_{id} - D_{Ii}^{-1}\hat{D}_i\gamma_i + \delta_i + w_i\right) + \frac{\dot{\tilde{\sigma}}_i\tilde{\sigma}_i}{\upsilon_i}\end{aligned} \qquad i = 4,5,6 \tag{49}$$

By Eqs. (34) and (41), Eq. (49) is transformed into

$$\begin{aligned}\dot{V}_i &= s_i\left(\ddot{q}_{id} - D_{Ii}^{-1}\hat{D}_i\left(\ddot{q}_{id} + w_i + \mu_{1i}s_i + \mu_{2i}sig(s_i)^{\beta} + k_i\,|w_i|\,\mathrm{sgn}\,(s_i)\right) + \delta_i + w_i\right) + \frac{\dot{\tilde{\sigma}}_i\tilde{\sigma}_i}{\upsilon_i} \\ &= s_i\left(\ddot{q}_{id} - D_{Ii}^{-1}D_{Ii}\,(1 + k_{2i}\sigma_i)\left(\ddot{q}_{id} + w_i + \mu_{1i}s_i + \mu_{2i}sig(s_i)^{\beta} + k_i\,|w_i|\,\mathrm{sgn}\,(s_i)\right) + \delta_i + w_i\right) + \frac{\dot{\tilde{\sigma}}_i\tilde{\sigma}_i}{\upsilon_i} \\ &= s_i\left(\ddot{q}_{id} - (1 + k_{2i}\sigma_i)\left(\ddot{q}_{id} + w_i + \mu_{1i}s_i + \mu_{2i}sig(s_i)^{\beta} + k_i\,|w_i|\,\mathrm{sgn}\,(s_i)\right) + \delta_i + w_i\right) + \frac{\dot{\tilde{\sigma}}_i\tilde{\sigma}_i}{\upsilon_i} \\ &= s_i\left(\delta_i - k_{2i}\sigma_i\ddot{q}_{id} - k_{2i}\sigma_i w_i - (1 + k_{2i}\sigma_i)\left(\mu_{1i}s_i + \mu_{2i}sig(s_i)^{\beta} + k_i\,|w_i|\,\mathrm{sgn}\,(s_i)\right)\right) + \frac{\dot{\tilde{\sigma}}_i\tilde{\sigma}_i}{\upsilon_i} \qquad i = 4,5,6 \\ &= s_i\left(\delta_{mi} - \mu_{m1i}s_i - \mu_{m2i}sig(s_i)^{\beta} - k_{2i}\sigma_i w_i - k_i(1 + k_{2i}\sigma_i)\,|w_i|\,\mathrm{sgn}\,(s_i)\right) + \frac{\dot{\tilde{\sigma}}_i\tilde{\sigma}_i}{\upsilon_i} \\ &= s_i\left(\delta_{mi} - \mu_{m1i}s_i - \mu_{m2i}|s_i|^{\beta}\mathrm{sgn}\,(s_i) - k_{2i}\sigma_i w_i - k_i(1 + k_{2i}\sigma_i)\,|w_i|\,\mathrm{sgn}\,(s_i)\right) + \frac{\dot{\tilde{\sigma}}_i\tilde{\sigma}_i}{\upsilon_i} \\ &= -\mu_{m1i}s_i^2 - \mu_{m2i}|s_i|^{\beta+1} + \delta_{mi}s_i - k_{2i}\sigma_i w_i s_i - k_i(1 + k_{2i}\sigma_i)\,|w_i|\,|s_i| + \frac{\dot{\tilde{\sigma}}_i\tilde{\sigma}_i}{\upsilon_i}\end{aligned} \tag{50}$$

where $\delta_{mi} = \delta_i - k_{2i}\sigma_i\ddot{q}_{id}$, $\mu_{m1i} = (1 + k_{2i}\sigma_i)\mu_{1i}$, $\mu_{m2i} = (1 + k_{2i}\sigma_i)\mu_{2i}$. Define k_i as

$$k_i = \frac{k_{2i}\sigma_i}{1 + k_{2i}\sigma_i} \tag{51}$$

Then $\dot{V}_i$ is

$$\dot{V}_i = -\mu_{m1i}s_i^2 - \mu_{m2i}|s_i|^{\beta+1} + \delta_{mi}s_i - k_{2i}\sigma_i w_i s_i - k_{2i}\sigma_i\,|w_i|\,|s_i| + \frac{\dot{\tilde{\sigma}}_i\tilde{\sigma}_i}{\upsilon_i} \qquad i = 4,5,6 \tag{52}$$

$\sigma_{i,\max}$ is a constant and $\tilde{\sigma}_i = \sigma_{i,\max} - \sigma_i$, so $\dot{\tilde{\sigma}}_i = -\dot{\sigma}_i$. $\sigma_i \geq 0$, $k_{2i} \geq 0$, then $k_{2i}\sigma_i w_i s_i + k_{2i}\sigma_i\,|w_i|\,|s_i| \geq 0$, $|\delta_{mi}|\,|s_i| \geq \delta_{mi}s_i$. So $\dot{V}_i$ satisfies

$$\dot{V}_i \leq -\,|s_i|\left(\mu_{m1i}\,|s_i| + \mu_{m2i}|s_i|^{\beta} - |\delta_{mi}|\right) - \frac{\tilde{\sigma}_i\dot{\sigma}_i}{\upsilon_i} \qquad i = 4,5,6 \tag{53}$$

Obviously $0 \leq \sigma_i \leq \sigma_{i,\max}$, so σ_i is bounded. According to the definition of TDE error Eq. (39), δ_{mi} is bounded. So assume $|\delta_{mi}| \leq \psi_i$, $\psi_i > 0$.

When $\frac{\tilde{\sigma}_i\dot{\sigma}_i}{\upsilon_i} \geq 0$, there are two scenarios. (a) $\sigma_i = \sigma_{i,\max} \vee \sigma_i = 0$ (b) $0 < \sigma_i < \sigma_{i,\max}$ and $|s_i|^{\alpha_{3i}} \leq \chi_i$. Then $\dot{V}_i$ is

$$\dot{V}_i \leq -\,|s_i|\left(\mu_{m1i}\,|s_i| + \mu_{m2i}|s_i|^{\beta} - |\delta_{mi}|\right) \tag{54}$$

When $\frac{\tilde{\sigma}_i\dot{\sigma}_i}{\upsilon_i} < 0$, obviously $0 < \sigma_i < \sigma_{i,\max}$ and $|s_i|^{\alpha_{3i}} > \chi_i$. Therefore, $\frac{\tilde{\sigma}_i\dot{\sigma}_i}{\upsilon_i} = -\tilde{\sigma}_i\,|s_i|$, then $\dot{V}_i$ is

$$\dot{V} \leq -\,|s_i|\left(\mu_{m1i}\,|s_i| + \mu_{m2i}|s_i|^{\beta} - |\delta_{mi}|\right) + \tilde{\sigma}\,|s_i| \tag{55}$$

https://doi.org/10.1017/S0263574722000108 Published online by Cambridge University Press

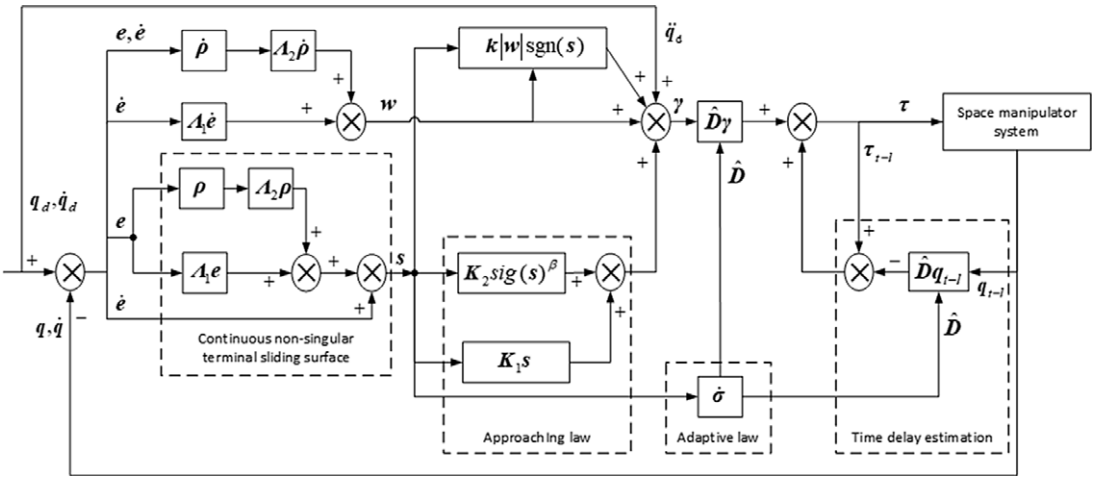


Figure 3. *The operational control strategy of the TDE-based adaptive sliding mode controller.*

Define $A_i = -|s_i|\left(\mu_{m1i}|s_i| + \mu_{m2i}|s_i|^{\beta} - |\delta_{mi}|\right) + \tilde{\sigma}_i|s_i|$, then A_i is rewritten as

$$A_i = -|s_i|\left[\left(\mu_{m1i} - (|\delta_{mi}| + \tilde{\sigma}_i)|s_i|^{-1}\right)|s_i| + \mu_{m2i}|s_i|^{\beta}\right] \tag{56}$$

$$A_i = -|s_i|\left[\mu_{m1i}|s_i| + \left(\mu_{m2i} - (|\delta_{mi}| + \tilde{\sigma}_i)|s_i|^{-\beta}\right)|s_i|^{\beta}\right] \tag{57}$$

When $s_i \neq 0$, either $(\mu_{m1i} - (|\delta_{mi}| + \tilde{\sigma}_i)|s_i|^{-1}) > 0$ or $(\mu_{m2i} - (|\delta_{mi}| + \tilde{\sigma}_i)|s_i|^{-\beta}) > 0$ satisfy. Then $A_i < 0$, so $\dot{V}_i < 0$, $\lim_{t\to\infty} e_i = 0$, $\lim_{t\to\infty} \dot{e}_i = 0$.

The operational control strategy of the proposed TDE-based adaptive sliding mode controller (42) is shown in Fig. 3.

5. Simulation examples

Simulations are carried out for a free-floating three-bar space manipulator, as shown in Fig. 1. The system's parameters are as follows: $m_0 = 1430\text{kg}$, $m_1 = 35\text{kg}$, $m_2 = 22.5\text{kg}$, $m_3 = 21.9\text{kg}$, $J_0 = 7090\text{kg}\cdot\text{m}^2$, $J_1 = 0.42\text{kg}\cdot\text{m}^2$, $J_2 = 0.94\text{kg}\cdot\text{m}^2$, $J_3 = 0.63\text{kg}\cdot\text{m}^2$, $l_0 = 0.5\text{m}$, $l_1 = 0.35\text{m}$, $l_2 = 0.87\text{m}$, $l_3 = 0.63\text{m}$, $b_1 = 0.25\text{m}$, $b_2 = 0.175\text{m}$, $b_3 = 0.315\text{m}$, $v = 1.2\text{m/s}$, $\theta_0 = -\frac{\pi}{6}rad$, $d = 2.3\text{m}$, $\theta_p = 242^{\circ}$, $\dot{x}_P = 0.95\text{m}/s$, $\dot{y}_P = -0.55\text{m}/s$, $\dot{\theta}_p = 0.13\text{rad/s}$, $[(\ddot{\boldsymbol{q}}_i)_{int}] = [0.05 \quad 0.05 \quad 0.05]^{\mathrm{T}}(^{\circ}/s^2)$.

Assume $L = 0.01\text{s}$, $t_0 = 0s$, $t_f = 66s$, $[\Delta v] = 0.02\text{m/s}$, $\xi(0) = [0.03\ 0.02\ 0.02]^{\mathrm{T}}$. The controller parameters are $\boldsymbol{D}_I = \text{diag}\,(1, 1, 1, 0.4, 0.3, 0.1)$, $\boldsymbol{\Lambda}_1 = \boldsymbol{\Lambda}_2 = \text{diag}\,(30, 30, 30, 30, 30, 30)$, $\boldsymbol{K}_1 = \text{diag}\,(2, 2, 2.4, 2, 2, 2.4)$, $\boldsymbol{K}_2 = \text{diag}(0.012, 0.012, 2.4, 0.012, 0.012, 2.4)$, $\alpha_{1i} = 0.8$, $\alpha_{2i} = 1.4$, $\alpha_{3i} = 2$, $\phi_i = 0.002$, $k_{1i} = 0.23$, $k_{2i} = 0.2$, $\zeta_{1i} = 0.5$, $\upsilon_i = 0.1$, $\chi_i = 0.1$, $\beta = 0.9$, $i = 1, \cdots, 6$.

Case 1 $\psi = -\frac{\pi}{6}rad$, $\phi = \frac{\pi}{3}$, the initial position of the base centroid relative to center of the target is $x_{C0}^{P} = -7.67m$, $y_{C0}^{P} = 1.77m$.

The simulation results of the RNS planning are shown in Figs. 4–7. Figure 4 shows the reactionless trajectories of the base centroid, the center of the end gripper. Figure 5 shows the reactionless joint trajectories, while Fig. 6 shows the reactionless joint angular accelerations. Figure 7 shows the reaction forces and reaction torque on the base.

The initial state is $\theta_1 = 0.56rad$, $\theta_2 = 1.43rad$, $\theta_3 = -1.92rad$, and the simulation results from the proposed controller Eq. (47) (controller II) are shown in Figs. 8–13. Figure 8 shows the actual trajectories of the base centroid, the center of the end gripper. Figure 9 is the actual trajectory of the base's attitude, while Fig. 10 depicts the tracking trajectories of joints. Figures 11, 12, and 13 are the estimators of

https://doi.org/10.1017/S0263574722000108 Published online by Cambridge University Press

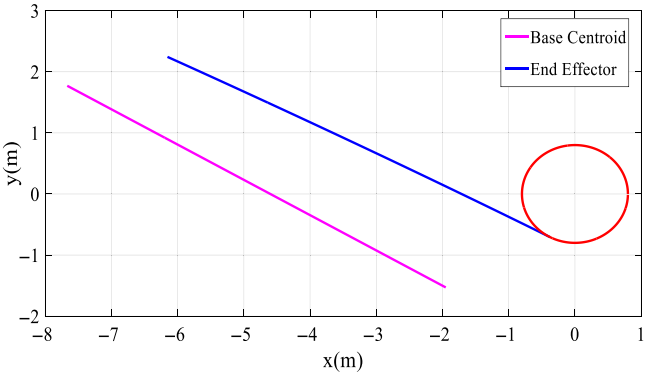


Figure 4. *The reactionless trajectories of the base centroid, the center of the end gripper (RNS planning,* $\psi = -\frac{\pi}{6} rad$*).*

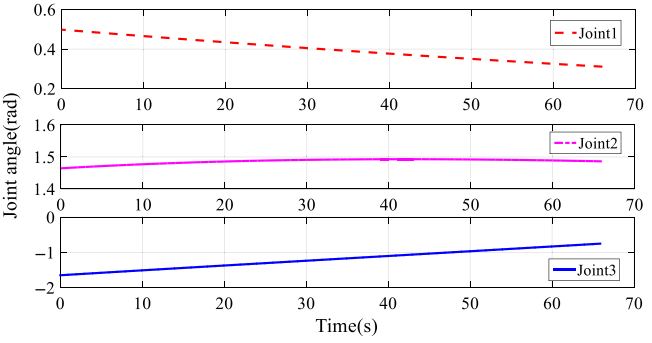


Figure 5. *The reactionless joint trajectories (RNS planning,* $\psi = -\frac{\pi}{6} rad$*).*

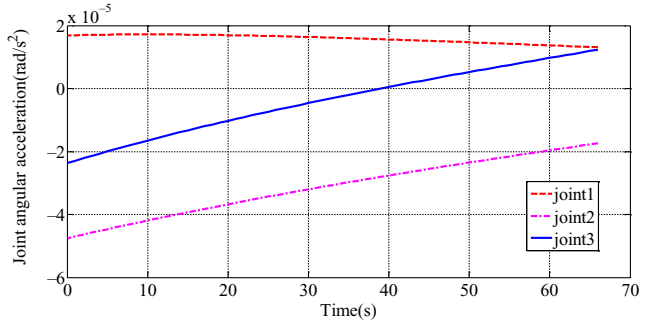


Figure 6. *The reactionless joint angular accelerations (RNS planning,* $\psi = -\frac{\pi}{6} rad$*).*

D_4, D_5, and D_6, respectively. When the end gripper comes into contact with the target handle, Δv is 0.0064 m/s. The simulation results from the controller Eq. (33) (controller I) are shown in Figs. 14–17. Figure 14 is the actual trajectory of the base's attitude, while Figs. 15–17 depict the tracking trajectories of joints 1–3, respectively.

Case 2 $\psi = -\frac{\pi}{9} rad$, $\phi = \frac{\pi}{3}$, the initial position of the base centroid relative to center of the target is $x_{C0}^P = -7.67m$, $y_{C0}^P = 0.34m$.

The simulation results of the RNS planning are shown in Figs. 18–21. Figure 18 shows the reactionless trajectories of the base centroid, the center of the end gripper. Figure 19 shows the reactionless joint trajectories, while Fig. 20 shows the reactionless joint angular accelerations. Figure 21 shows the reaction forces and the reaction torque on the base.

https://doi.org/10.1017/S0263574722000108 Published online by Cambridge University Press

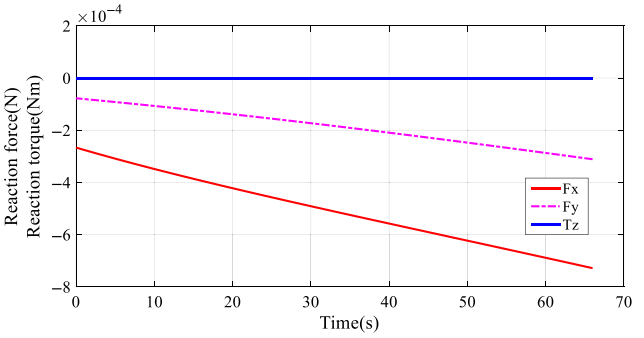


Figure 7. *The reaction forces (RNS planning, $\psi = -\frac{\pi}{6} rad$).*

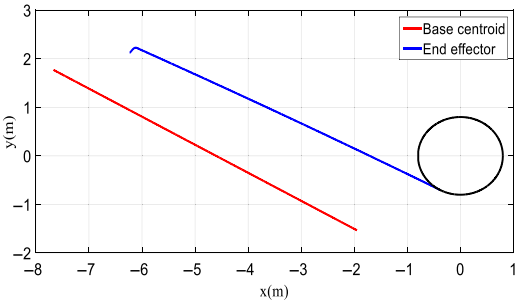


Figure 8. *The actual trajectories of the base centroid, the center of the end gripper ($\psi = -\frac{\pi}{6} rad$, controller II).*

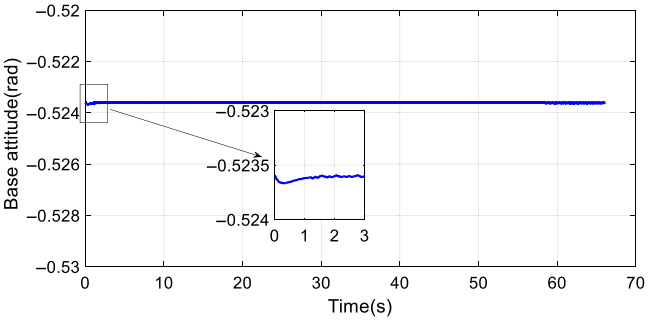


Figure 9. *The tracking trajectory of the base's attitude ($\psi = -\frac{\pi}{6} rad$, controller II).*

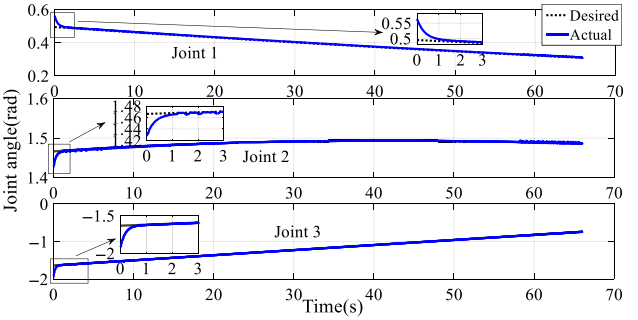


Figure 10. *The tracking trajectory of joints ($\psi = -\frac{\pi}{6} rad$, controller II).*

https://doi.org/10.1017/S0263574722000108 Published online by Cambridge University Press

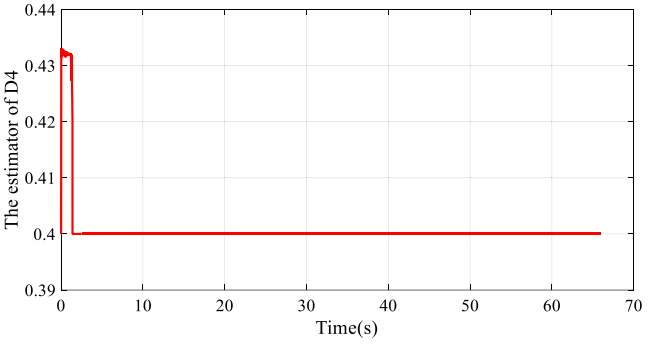


Figure 11. *The estimator of D_4 ($\psi = -\frac{\pi}{6} rad$, controller II).*

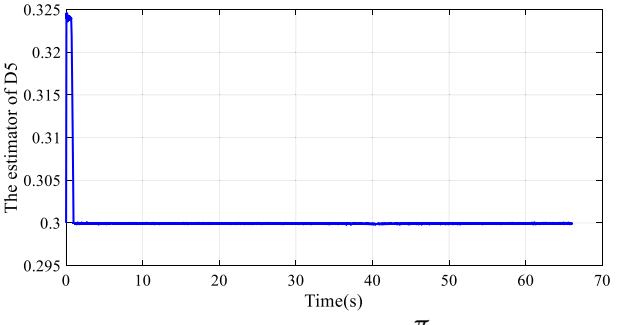


Figure 12. *The estimator of D_5 ($\psi = -\frac{\pi}{6} rad$, controller II).*

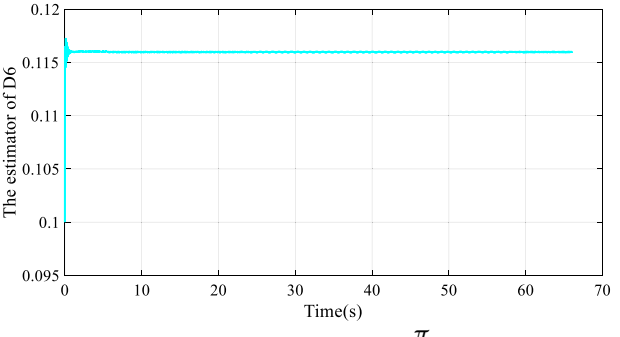


Figure 13. *The estimator of D_6 ($\psi = -\frac{\pi}{6} rad$, controller II).*

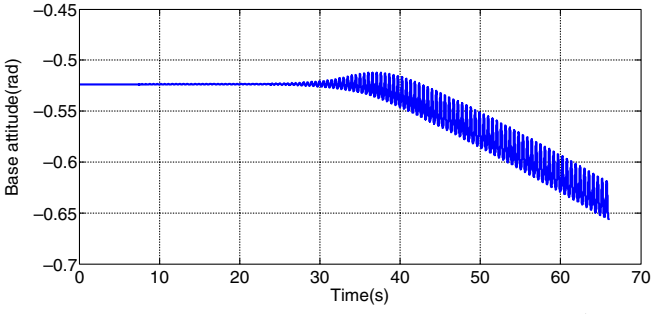


Figure 14. *The tracking trajectory of the base's attitude ($\psi = -\frac{\pi}{6} rad$, controller I).*

https://doi.org/10.1017/S0263574722000108 Published online by Cambridge University Press

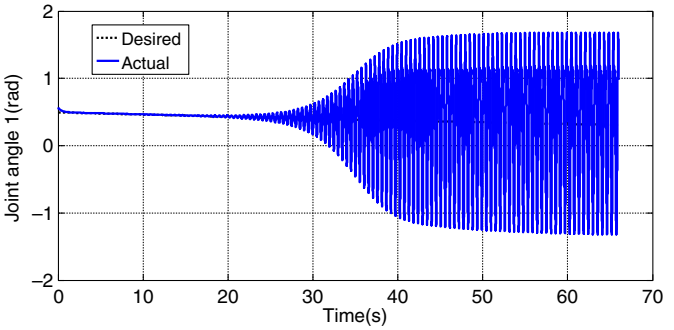


Figure 15. *The tracking trajectory of joint 1 ($\psi = -\frac{\pi}{6} rad$, controller I).*

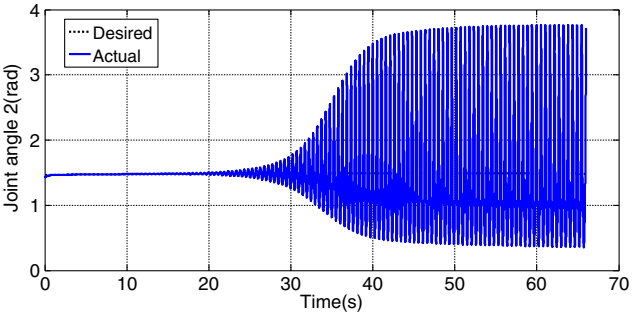


Figure 16. *The tracking trajectory of joint 2 ($\psi = -\frac{\pi}{6} rad$, controller I).*

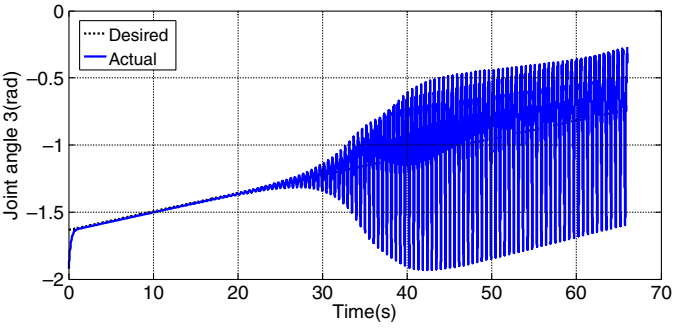


Figure 17. *The tracking trajectory of joint 3 ($\psi = -\frac{\pi}{6} rad$, controller I).*

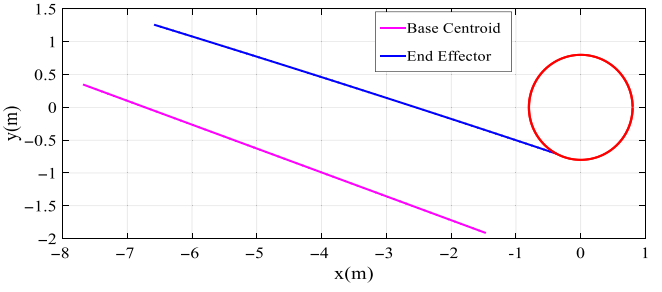


Figure 18. *The reactionless trajectories of the base centroid, the center of the end gripper (RNS planning, $\psi = -\frac{\pi}{9} rad$).*

https://doi.org/10.1017/S0263574722000108 Published online by Cambridge University Press

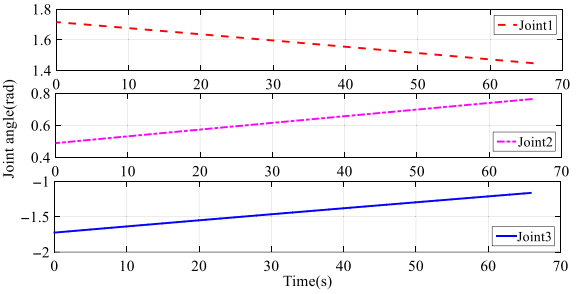


Figure 19. *The reactionless joint trajectories (RNS planning,* $\psi = -\frac{\pi}{9} rad$*).*

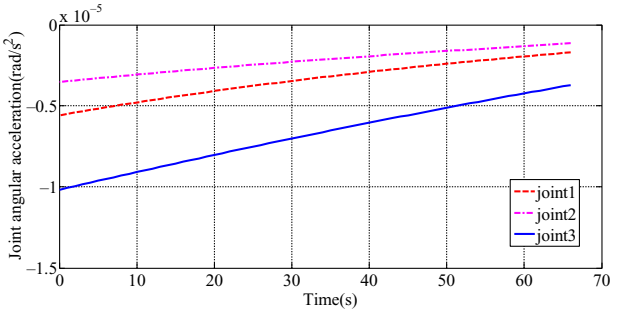


Figure 20. *The reactionless joint angular accelerations (RNS planning,* $\psi = -\frac{\pi}{9} rad$*).*

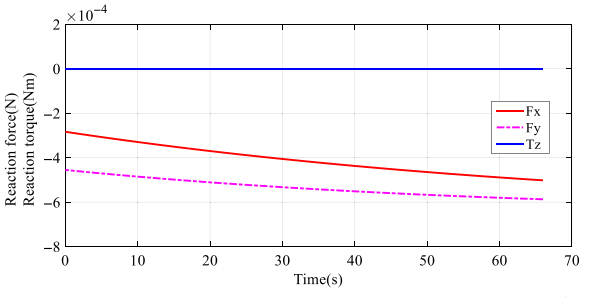


Figure 21. *The reaction forces (RNS planning,* $\psi = -\frac{\pi}{9} rad$*).*

The initial state is $\theta_1 = 1.79 rad$, $\theta_2 = 0.40 rad$, $\theta_3 = -1.90 rad$, and the simulation results from the proposed controller Eq. (47) (controller II) are shown in Figs. 22–27. Figure 22 shows the actual trajectories of the base centroid, the center of the end gripper. Figure 23 is the actual trajectory of the base's attitude, while Fig. 24 depicts the tracking trajectories of joints. Figures 25, 26, and 27 are the estimators of D_4, D_5, and D_6, respectively. When the end gripper comes into contact with the target handle, Δv is 0.0192 m/s. The simulation results from the controller Eq. (33) (controller I) are shown in Figs. 28–31. Figure 28 is the actual trajectory of the base's attitude, while Figs. 29–31 depict the tracking trajectories of joints 1–3, respectively.

Figures 6 and 20 show that the reactionless joint angular accelerations are less than their allowable values, and Figs. 7 and 21 show that the reaction forces and reaction torque on the base are almost 0. It can be seen from Figs. 9 and 23 that the base's attitude changes slightly at the beginning, and then remains to be $-\frac{\pi}{6} rad$ by the controller II. Meanwhile, it can be seen from Figs. 10 and 24 that the joint angles gradually track the desired reactionless trajectories and that the errors converge to zero after

https://doi.org/10.1017/S0263574722000108 Published online by Cambridge University Press

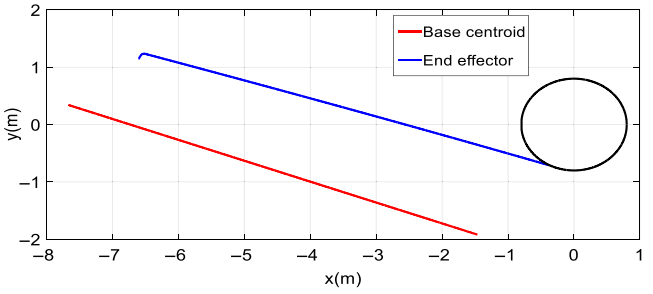


Figure 22. *The actual trajectories of the base centroid, the center of the end gripper ($\psi = -\frac{\pi}{9} rad$, controller II).*

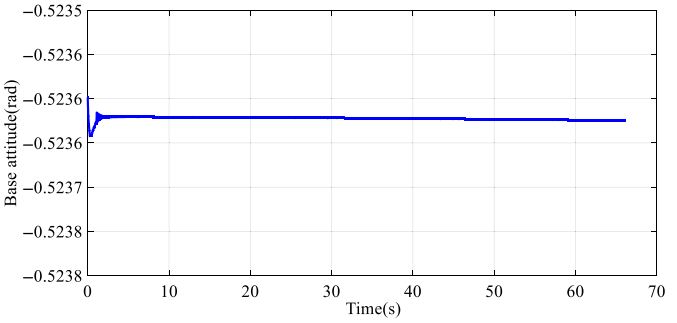


Figure 23. *The tracking trajectory of the base's attitude ($\psi = -\frac{\pi}{9} rad$, controller II).*

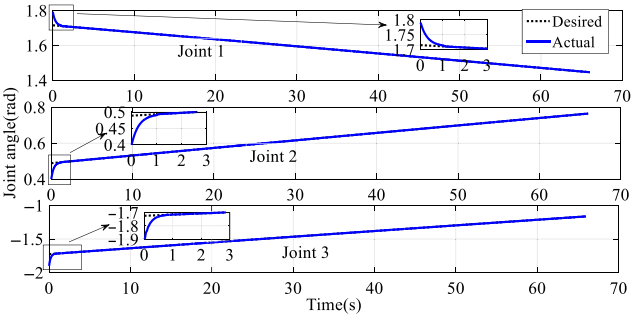


Figure 24. *The tracking trajectories of joints ($\psi = -\frac{\pi}{9} rad$, controller II).*

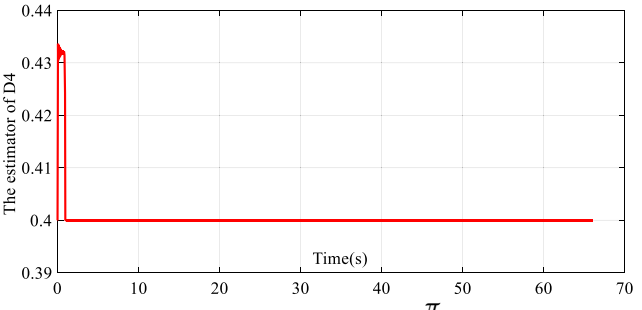


Figure 25. *The estimator of D_4 ($\psi = -\frac{\pi}{9} rad$, controller II).*

https://doi.org/10.1017/S0263574722000108 Published online by Cambridge University Press

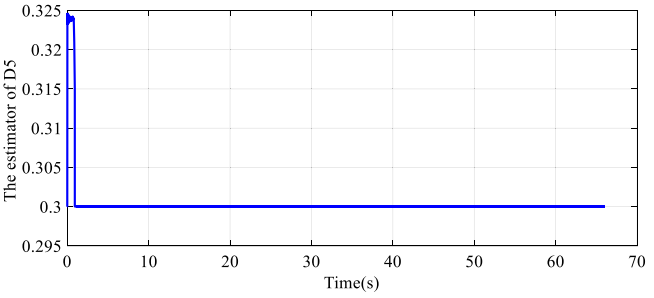


Figure 26. *The estimator of D_5 ($\psi = -\frac{\pi}{9} rad$, controller II).*

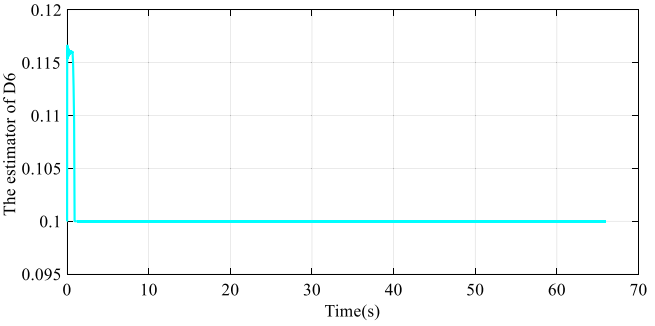


Figure 27. *The estimator of D_6 ($\psi = -\frac{\pi}{9} rad$, controller II).*

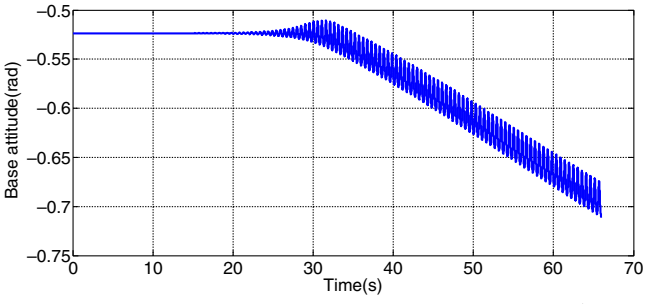


Figure 28. *The tracking trajectory of the base's attitude ($\psi = -\frac{\pi}{9} rad$, controller I).*

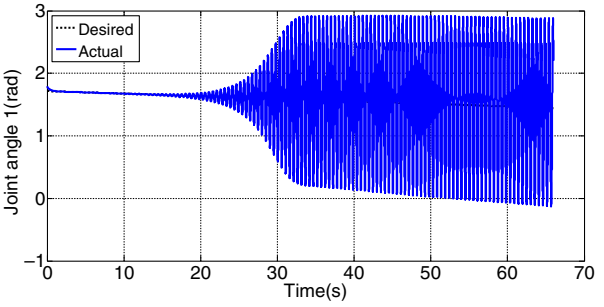


Figure 29. *The tracking trajectory of joint 1 ($\psi = -\frac{\pi}{9} rad$, controller I).*

https://doi.org/10.1017/S0263574722000108 Published online by Cambridge University Press

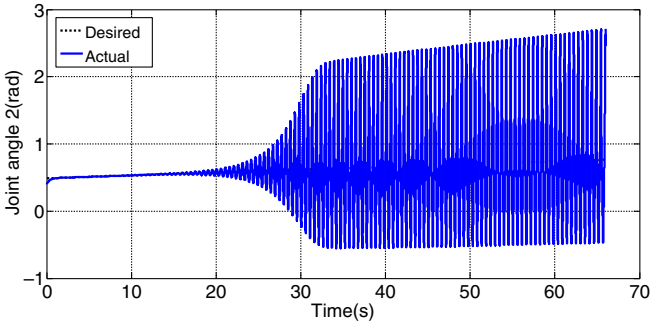


Figure 30. *The tracking trajectory of joint 2 ($\psi = -\frac{\pi}{9} rad$, controller I).*

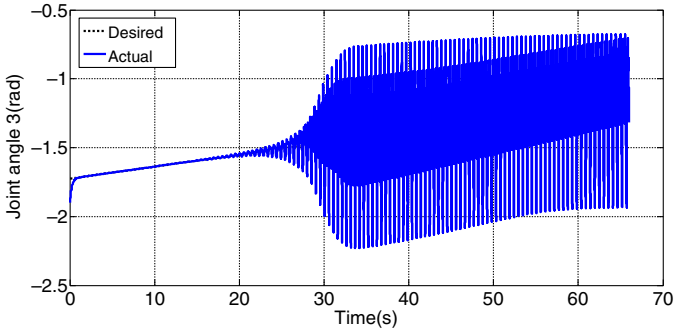


Figure 31. *The tracking trajectory of joint 3 ($\psi = -\frac{\pi}{9} rad$, controller I).*

about 2 s by the controller II. From Figs. 14–17 and 28–31, it can be seen serious chattering happens after 20 s, and the reactionless desired joint trajectories cannot be tracked efficiently by the controller I .

6. Conclusions

The Lagrange dynamic model of a free-floating three-bar space manipulator was established. The RNS motion planning algorithm of the manipulator's pregrasping a rotating target was derived, and the vector norm constraint algorithm of RNS planning was addressed. Then an augmented adaptive sliding mode controller based on TDE was proposed, in which the adaptive estimated inertia matrix was introduced to decrease the estimation errors and avoid serious chattering and accurate dynamics were not required. The proposed RNS planning algorithm and the proposed controller ensured that joint angular accelerations were less than their allowable values and each joint tracked the desired reactionless trajectory with the base's attitude reactionless.

Acknowledgments. This work was supported by the National Natural Science Foundation of China (grant number 51741502), the Natural Science Foundation of Fujian Province (grant number 2020J01450), and Fujian Provincial Industrial Robot Basic Components'Technology Research Platform (grant number 2014H21010011).

Author Contributions. Xiaoyan Yu conceived and designed the study. Xiaoyan Yu and Jianyu Zhang performed simulations. Xiaoyan Yu and Jianqiao Guo derived the dynamic equations and wrote the article.

Conflicts of Interests. The authors declare none.

https://doi.org/10.1017/S0263574722000108 Published online by Cambridge University Press

References

[1] X. L. Ding, Y. C. Wang, Y. B. Wang and K. Xu, "A review of structures, verification, and calibration technologies of space robotic systems for on-orbit servicing," *Sci. China (Technol. Sci.)* **64**(03), 462–480 (2021).

[2] E. Papadopoulos, F. Aghili, O. Ma and R. Lampariello, "Robotic manipulation and capture in space: A survey," *Front. Rob. AI* 8 (2021).

[3] L. J. Zong and M. R. Emami, "Control verifications of space manipulators using ground platforms," *IEEE Trans. Aerospace Electron. Syst.* **1**(57), 341–354 (2021).

[4] A. Seddaoui and C. M. Saaj, "Combined nonlinear H∞ controller for a controlled-floating space robot," *J. Guid. Control. Dyn.* **42**(8), 1878–1885 (2019).

[5] H. S. Jayakody, L. Shi, J. Katupitiya and N. Kinkaid, "Robust adaptive coordination controller for a spacecraft equipped with a robotic manipulator," *J. Guid. Control. Dyn.* **39**(12), 2699–2711 (2016).

[6] J. Cheng and L. Chen, "Coordinated robust control based on extended state observer of dual-arm space robot with closed chain for transferring a target," *Proc. Inst. Mech. Eng. Part G J. Aerosp. Eng.* **232**(13), 2489–2498 (2018).

[7] T. Rybus, "Point-to-point motion planning of a free-floating space manipulator using the rapidly-exploring random trees (RRT) method," *Robotica.* **38**(6), 957–982 (2020).

[8] S. Dubowsky and E. Papadopoulos, "The kinematics, dynamics, and control of free-flying and free-floating space robotic systems," *IEEE Trans. Robot. Autom.* **9**(5), 531–543 (1993).

[9] S. Dubowsky and M. A. Torres, "Path Planning for Space Manipulators to Minimize Spacecraft Attitude Disturbances," *Proceedings. 1991 IEEE International Conference on Robotics and Automation*, Sacramento, CA, USA (1991) pp. 2522–2538.

[10] D. Nenchev, Y. Umetani and K. Yoshida, "Analysis of a redundant free-flying spacecraft/manipulator system," IEEE Trans. Robot. *Autom.* **8**(1), 1–63 (2002).

[11] K. Yoshida, K. Hashizume and S. Abiko, "Zero Reaction Maneuver: Flight Validation with ETS-VII Space Robot and Extension to Kinematically Redundant Arm," *Proceedings of the IEEE International Conference on Robotics and Automation*, Seoul, Korea (2001) pp. 441–446.

[12] K. Yoshida, "Engineering Test Satellite VII flight experiments for spacerobot dynamics and control: Theories on laboratory test beds ten years ago, now in orbit," *Int. J. Rob. Res.* **22**(5), 321–335 (2003).

[13] Y. Fukazu, N. Hara, Y. Kanamiya and D. Sato, "Reactionless Resolved Acceleration Control with Vibration Suppression Capability for JEMRMS/SFA," *Proceedings of the IEEE International Conference on Robotics and Biomimetics*, Bangkok, Thailand (2009) pp. 1359–1364.

[14] T. C. Nguyen Huynh and I. Sharf, "Adaptive reactionless motion and parameter identification in post-capture of space debris," *J. Guidance Control Dyn.* **36**(2), 404–414 (2013).

[15] S. F. Xu, H. L. Wang, D. Z. Zhang and B. H. Yang, "Adaptive Reactionless Motion Control for Free-Floating Space Manipulators with Uncertain Kinematics and Dynamics," *The 3rd IFAC International Conference on Intelligent Control and Automation Science*, Chengdu, China (2013).

[16] L. J. Zong, M. R. Emami, J. J. Luo and J. J. Luo, "Reactionless control of free-floating space manipulators," *IEEE Trans. Aerospace Electron. Syst.* **56**(2), 1490–1503 (2020).

[17] S. Ding, J. Wang and W. X. Zheng, "Second-order sliding mode control for nonlinear uncertain systems bounded by positive functions," *IEEE Trans. Ind. Electron.* **62**(9), 5899–5909 (2015).

[18] A. Nasiri, S. Kiong Nguang and A. Swain, "Adaptive sliding mode control for a class of MIMO nonlinear systems with uncertainties," *J. Franklin Inst.* **351**(4), 2048–2061 (2014).

[19] H. Alwi and C. Edwards, "Sliding mode fault-tolerant control of an octorotor using linear parameter varying-based schemes," *IET Control Theory Appl.* **9**(4), 618–636 (2015).

[20] X. T. Tran and H. J. Kang, "Adaptive hybrid high-Order terminal sliding mode control of MIMO uncertain nonlinear systems and application to robot manipulators," *Int. J. Precis. Eng. Manuf.* **16**(2), 255–266 (2015).

[21] R. Su and Q. Zong, "Comprehensive design of disturbance observer and non-singular terminal sliding," *IET Control Theory App.* **9**(12), 1821–1830 (2015).

[22] A. Al-Ghanimi, Z. H. Man and J. C. Zheng, "Robust and fast non-singular terminal sliding mode control for piezoelectric actuators," *IET Control Theory Appl.* **9**(18), 2678–2687 (2015).

[23] X. Y. Yu, "Hybrid-trajectory based terminal sliding mode control of a flexible space manipulator with an elastic base," *Robotica.* **38**(3), 550–563 (2020).

[24] F. Bayat, "Model predictive sliding control for finite-time three-axis spacecraft attitude tracking," *IEEE Trans. Ind. Electron.* **66**(10), 7986–7996 (2019).

[25] X. Shao, G. Sun, C. Xue and X. Li, "Nonsingular terminal sliding mode control for free-floating space manipulator with disturbance," *Acta Astronautica.* **181**, 396–404 (2021).

[26] Y. K. Zhu, J. Z. Qiao and L. Guo, "Adaptive sliding mode disturbance observer-based composite control with prescribed performance of space manipulators for target capturing," *IEEE Trans. Ind. Electron.* **66**(3), 1973–1983 (2019).

[27] ,Y. Y. Wang, J. W. Chen, L. Y. Gu and X. D. Li, "Time delay control of hydraulic manipulators with continuous nonsingular terminal sliding mode," *J. Cent. South Univ.* **22**(12), 4616–4624 (2015).

[28] X. L. X. Liang, Y. W. Y. Wan, C. Z. C. Zhang, Y. Y. Kong, Q. Q. Xin and W. Yi, "Robust position control of hydraulic manipulators using time delay estimation and nonsingular fast terminal sliding mode," *Proc. Inst. Mech. Eng. Part I J. Syst. Control Eng.* **232**(1), 50–61 (2018).

[29] P. H. Chang and S. H. Park, "On improving time-delay control under certain hard nonlinearities," *Mechatronics.* **13**(4), 393–412 (2003).

https://doi.org/10.1017/S0263574722000108 Published online by Cambridge University Press

[30] Y. Y. Wang, G. SH. Luo, L. Y. Gu, and X. D. Li, "Fractional-order nonsingular terminal sliding mode control of hydraulic manipulators using time delay estimation," *JVC/Journal Vib. Control.* **22**(19), 3998–4011 (2016).
[31] J. Lee, C. Yoo, Y. Park, B. B. Park, S. J. Lee, D. G. Gweon and P. H. Chang, "An experimental study on time delay control of actuation system of tilt rotor unmanned aerial vehicle," *Mechatronics.* **22**(2), 184–194 (2012).
[32] B. Brahmi, M. Driscoll, M. H. Laraki and A. Brahmi, "Adaptive high-order sliding mode control based on quasi-time delay estimation for uncertain robot manipulator," *Control Theory Technol.* **18**(3), 279–292 (2020).
[33] Y. Y. Wang, Y. Fei, S. R. Jiang and B. Chen, "Adaptive nonsingular terminal sliding mode control of cable-driven manipulators with time delay estimation," *Int. J. Syst. Sci.* **51**(8), 1429–1447 (2020).
[34] S. Jung and J. W. Lee, "Similarity analysis between a nonmodel-based disturbance observer and a time-delayed controller for robot manipulators in cartesian space," *IEEE Access.* **9**, 122299–122307 (2021).
[35] J. Y. Zhang, X. Y. Yu and L. Chen, "Terminal sliding mode adaptive fuzzy controller of a free-floating space manipulator based on time delay estimation," *Mech. Mach. Sci.* **79**, 440–449 (2020).
[36] J. Liang, "Fuzzy Wavelet Neural Network Control of Joint Flexible Double-Arm Space Robot Based on Delay Estimation," *The Chinese Congress of Theoretical and Applied Mechanics (CCTAM 2015)*, Shanghai, China (2015) pp. 249–249.
[37] Z. C. Xie, T. Sun and X. F. Wu, "A new reinforcement learning based adaptive sliding mode control scheme for free-floating space robotic manipulator," *IEEE Access.* **8**, 127048–127064 (2020).
[38] L. J. Zong, M. R. Emami and J. J. Luo, "Reactionless control of free-floating space manipulators," *IEEE Trans.* Aerospace Electron. *Syst.* **56**(2), 1490–1503 (2020).
[39] Q. Song, "Reactionless sliding mode fault tolerant control of floating space manipulator," Fuzhou University (2020).
[40] X. Y. Yu, J. Q. Guo and J. Y. Zhang, "Reactionless Time Delay Estimation Based Adaptive Fuzzy Sliding Mode Control of a Space Manipulator Approaching a Rotating Target," *International Astronautical Congress 2021*. Dubai, the United Arab Emirates (2021).
[41] S. Cho, J. Baek and S. Han, "Practical time-delay control with adaptive gains for trajectory tracking of robot manipulators," *IEEE Trans. Ind. Electron.* **65**(7), 5682–5692 (2018).

Cite this article: X. Y. Yu, J. Q. Guo and J. Y. Zhang (2022). "Time delay estimation-based reactionless augmented adaptive sliding mode control of a space manipulator's pregrasping a target", Robotica **40**, 3136–3156. https://doi.org/10.1017/S0263574722000108

https://doi.org/10.1017/S0263574722000108 Published online by Cambridge University Press